On spallation of EB-PVD thermal barrier coatings on turbine blades

Christopher M. Harvey[1], Simon Wang[1,2,*], Bo Yuan[1],
Rachel C. Thomson[3] and Gary W. Critchlow[3]

[1] Department of Aeronautical and Automotive Engineering,
Loughborough University, Loughborough, Leicestershire LE11 3TU, UK
[2] College of Mechanical and Equipment Engineering,
Hebei University of Engineering, Handan 056038, China
[3] Department of Materials Engineering,
Loughborough University, Loughborough, Leicestershire LE11 3TU, UK

Abstract. Room temperature blistering and spallation failures reduce the life time of thermal barrier coatings (TBC). Based on the theory of pockets of energy concentration, a mechanical model for the multilayer circular blister is presented, considering the variable material properties through the coating thickness. Conditions are revealed analytically for nucleation, propagation and the spallation of TBC blisters. The predictions from the mechanical model on radii for TBC blister unstable growth and spallation are in good agreement with experimental results. Furthermore, this model is beneficial to determine the interface fracture toughness and the residual stress in the coating system.

Keywords: Composite materials, Interface fracture, Pockets of energy concentration, Spallation, Thermal barrier coatings.

1 Introduction

Thermal barrier coatings (TBC) are multilayer composite material systems applied in aero engine components to withstand high and prolonged heat loads. TBCs may degrade and spall during service, exposing the substrate to elevated temperatures, resulting in oxidation and ultimately metal loss. A related failure is the TBC room-temperature spallation under the constant in-plane residual stress after cooling. In experiments, microscopic fractographs manifest possible reasons for the observed spallation, including voids generated in the thermally grown oxides (TGO) due to the compromised oxidation of aluminum and titanium, migration of sulfur from the substrate to the interface, minor morphologic defects at interfaces of TGO during manufacturing, TGO imprints on the substrate as a result of the interface creeping and TGO grain growth on uneven interfacial boundaries, mixed oxides underneath the pure alumina due to the exhaustion of aluminum in the bond coat, phase transformation such as β phase with bcc crystal structure transforms to γ and γ' phase with fcc crystal structure, etc.

In the mechanical viewpoint, Wang, Harvey et al. [1,2] recently reported that pockets of energy concentration (PECs) exist in the form of pockets of tensile stress and shear

* Corresponding author, E-mail: s.wang@lboro.ac.uk (Simon Wang)

stress in and around the interface between the TGO and the substrate. It is hypothesized that PECs can be caused by dynamic and non-uniform plastic relaxation, creep, or chemical reactions in thermal cycles as aforementioned. The mechanical models revealed a new spallation mechanism: PECs supply the blister energy, driving blisters nucleate, grow and spall. The analytical results reach excellent agreement with the experimental measurements from Refs. [3,4] for the spallation of α-alumina blisters.

The PECs hypothesis has essential differences from the buckling-driven approach: (1) The PECs approach is a pure energy balance approach whereby blister growth is driven by an energy source in addition to the constant residual stress; whereas in the buckling-driven approach, the compressive residual stress is required to rise to a critical level for blister growth. (2) With PECs, the blister automatically bends away from the substrate; however, with the buckling-driven approach, at the buckling radius the initial separation has no amplitude and the ERR is zero. (3) With PECs, the blister arc length increases as the blister bends away from the substrate; whereas, a constant arc length is assumed under the buckling-driven approach.

This paper aims to develop a mechanical model based on the PECs theory [3,4], for the multilayer circular blister that nucleates, grows and spalls off from a relatively thick substrate. The mechanical model is then verified with the spallation radius measurement in the experiment for the electro-beam physical vapor deposition (EB-PVD) TBCs with the γ/γ′ bond coat.

2 Analytical mechanical model for blisters with circular edges

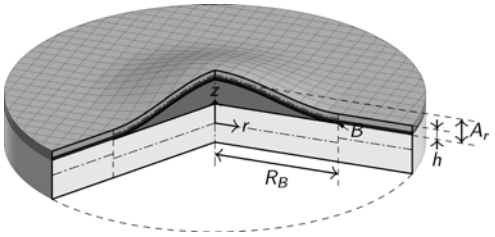

Fig. 1. A multilayer blister with the circular edge.

Fig. 1 shows a multilayer circular blister with the thickness h, blister radius R_B and the blister height A_r. The subscript B denotes the cracking edges. As per the PECs theory [1,2], the blister energy $(U_a)_{GR}$ for a growing blister is

$$(U_a)_{GR} = \pi R_B^2 \left\{ G_c \left(1 + \frac{AD - B^2}{2AD} \right) + \frac{3A\varepsilon_0^3}{2\pi^2 \Omega^*} \left(\frac{R_B}{h} \right)^2 \left[\frac{3\varepsilon_0}{\pi^2 \Omega^*} \left(\frac{R_B}{h} \right)^2 - 2\frac{A^*}{A} \right] \right\} \tag{1}$$

where $A = \int_{-h/2}^{h/2} E(z) / \left[1 - \nu^2(z) \right] dz$ and $A^* = \int_{-h/2}^{h/2} E(z) / \left[1 - \nu(z) \right] dz$ are extensional stiffnesses, $B = \int_{-h/2}^{h/2} E(z) / \left[1 - \nu^2(z) \right] z\, dz$ is the coupling stiffness,

$D=\int_{-h/2}^{h/2}E(z)/\left[1-\nu^2(z)\right]z^2dz$ is the bending stiffness, ε_0 is the biaxial residual strain, and $G_c=G_{Ic}$ based on the classical plate partition theory [5–7]. The Ω^* is

$$\Omega^*=\frac{A^*\varepsilon_0^2}{G_{cE}}\frac{6AD^2}{A^*\left(AD-B^2\right)h^2}=\frac{A^*\varepsilon_0^2}{G_c}\Delta \tag{2}$$

where $A^*\varepsilon_0^2/G_c$ is the ratio between the biaxial residual strain energy density and the interface toughness while $\Delta=6AD^2/\left[A^*\left(AD-B^2\right)h^2\right]$ is a constant factor independent of energy release rate (ERR) partition theories. From Eq. (1), Ω^* plays a key role in blister development. Note $\Omega^*=\Omega/(1+\nu)^2$ in the isotropic material system, where $\Omega=hE\varepsilon_0^2(1+\nu)/\left[2(1-\nu)G_c\right]$ [1,2].

In the mechanical viewpoint [1,2], PECs drive the blister nucleate and develop relatively slowly and steadily first under the constant in-plane residual stress within the blister, then along with the increase of the blister height and the blister radius, buckling happens and drives the unstable growth of the blister. The blister energy describing the net energy stored in the developing blister is supplied by the PECs and increases to reach the maximum value, behind which no more PECs will be stored in the blister. After that, the blister continues growing with the crack extending since the ERRs at crack tips are larger than the fracture toughness. In the meanwhile, the restored blister energy in the stable and unstable growth stages transforms to the kinetic energy, with a relatively abrupt growth of the blister. Eventually, spallation happens with the blister energy is exhausted.

The radii for the unstable growth (denoted by UG) and the spallation (denoted by SP) of the blister are expressed in Eqs. (3) and (4), respectively.

$$\left(\frac{R_B}{h}\right)_{UG}^2=\frac{\pi^2\Omega^*A^*}{6\varepsilon_0A}\left\{1-\left[1-\frac{\alpha^2}{\Omega^*}\left(\frac{A}{A^*}\right)^2\right]^{1/2}\right\} \tag{3}$$

$$\left(\frac{R_B}{h}\right)_{SP}^2=\frac{\pi^2\Omega^*A^*}{3\varepsilon_0A}\left\{1-\left[1-2\frac{A}{A^*\Omega^*}\left(\frac{3D}{A^*h^2}+\Delta\right)\right]^{1/2}\right\} \tag{4}$$

For $\Omega^*>>\left(\alpha A/A^*\right)^2$, Eq. (3) can be written as

$$\left(\frac{R_B}{h}\right)_{UG}^2=\frac{(\pi\alpha)^2}{12\varepsilon_0}\frac{A}{A^*} \tag{5}$$

From Eq. (4), the blister will not spall for $\Omega^*<2A\left[3D/\left(A^*h^2\right)+\Delta\right]/A^*$; however, for $\Omega^*>>2A\left[3D/\left(A^*h^2\right)+\Delta\right]/A^*$, Eq. (4) can be approximated as

$$\left(\frac{R_{\mathrm{B}}}{h}\right)^2_{\mathrm{SP}} = \frac{\pi^2}{3\varepsilon_0}\left(\frac{3D}{A^* h^2} + \Delta\right) \tag{6}$$

The above equations can be equally applied for either classical plate partition theory (denoted by E) [5–7] or first-order shear-deformable plate partition theory (denoted by T) [5–7] or 2D elasticity plate partition theory (denoted by 2D) [8–10]. However, the interface fracture toughness G_{c} needs to be taken as $G_{\mathrm{c}} = G_{\mathrm{Ic}}$, $G_{\mathrm{c}} = \psi\psi_{\mathrm{IT}} G_{\mathrm{Ic}} / \left(\psi + \psi_{\mathrm{IT}} - 1\right)$ and $G_{\mathrm{c}} = \psi\psi_{\mathrm{I2D}} G_{\mathrm{Ic}} / \left(\psi + \psi_{\mathrm{I2D}} - 1\right)$ respectively for the three partition theories, where G_{Ic} is the critical mode I fracture toughness and $G_{\mathrm{IIc}} = \psi G_{\mathrm{Ic}}$, $G_{\mathrm{IT}} / G_{\mathrm{cT}} = 4\left(AD - B^2\right) \Big/ \left[A\left(Ah^2 + 4Bh + 4D\right)\right] = 1/\psi_{\mathrm{IT}}$ and $G_{\mathrm{I2D}} / G_{\mathrm{c2D}} = 0.6227\left[12\left(AD - B^2\right) \Big/ \left(A^2 h^2\right)\right] = 1/\psi_{\mathrm{I2D}}$.

3 Experimental validation

The mechanical model for multilayer material system is verified with the experimental measurements for EB-PVD TBC spallation at the room temperature. Experimental observations show the spalled coating consists of the ceramic top coat and the TGO. The experimental details are presented in Ref. [11].

The task is comparing the analytical predications with the experimental measurements in Ref. [11]. The thickness of the top coat and the TGO are 138 μm and 5 μm, respectively. The through-thickness variation of Young's modulus for the top coat is based on the experiment for the same TBC structure isothermally ageing 120 hours at 1150 °C [12], that is a polynomial fit used: $E_{\mathrm{TC}} = -8 \cdot 10^{-5} z_{\mathrm{TC}}^3 + 0.0192 z_{\mathrm{TC}}^2 - 1.5812 z_{\mathrm{TC}} + 85.585$ GPa, where z_{TC} is in microns, $z_{\mathrm{TC}} = 0$ is at the bottom of the top coat and positive upward, and the Poisson's ratio is $\nu_{\mathrm{TC}} = 0.2$ [13]. For the TGO, the Young's modulus and Poisson's ratio are $E_{\mathrm{TGO}} = 400$ GPa and $\nu_{\mathrm{TGO}} = 0.25$ [13,14], respectively. The mismatch in thermal expansion between the TGO and the Ni-substrate is 4 ppm/°C [15]. For a temperature difference of 1110 °C, the biaxial compressive residual strain is 0.444 %. The mode-I fracture toughness at the interface between the TGO and bond coat is 8.4 Jm^{-2} [15] and the fracture toughness ratio ψ is 5 [16]. Note that $\Delta = 0.522$ in Eq. (2), which is independent on the partition theories. The Ω^* values based on the E, T and 2D theories are 20.724, 9.698 and 16.296, respectively, which are larger than $\left(\alpha A / A^*\right)^2$ required by Eq. (3) and larger than $2A\left[3D / \left(A^* h^2\right) + \Delta\right] / A^*$ required by Eq. (4).

Then the Eqs. (3) and (5) are used to assess the initiation of the blister unstable growth, and Eqs. (4) and (6) are for the coating spallation radius, and the results are summarized in Table 1.

Table 1. Circular blister radius comparison for the initiation of unstable growth and spallation.

	Initiation of unstable growth R_B (mm)					Spallation R_B (mm)				
	Eq. (3)			Eq. (5)		Eq. (4)			Eq. (6)	
α	E	T	2D	All	Test data	E	T	2D	All	Test data
0.652	1.16	1.16	1.16	1.15	1.1±0.1 Ref. [11]	3.45	3.49	3.46	3.43	3.3±0.1 Ref. [11]
0.936	1.66	1.67	1.67	1.66						
1.22	2.17	2.19	2.18	2.16						

The measured radius of the initiation of the unstable growth is very close to the analytical prediction (minimum 4.5 % difference) if taking $\alpha = 0.652$ and is far smaller than 2.16 mm that is usually assumed in the conventional buckling approach from Eq. (2) with $\alpha = 1.220$. Since the values of Ω^* are much larger than $\left(\alpha A/A^*\right)^2$ required by Eq. (3) and larger than $2A\left[3D/\left(A^*h^2\right)+\Delta\right]/A^*$ required by Eq. (4). Hence, Eqs. (5) and (6) give good approximations. In the comparison of the spallation radius, again, the predictions are close to the experimental results (minimum 3.9 % difference). This excellent comparison clearly confirms the new spallation failure mechanism of multilayer materials such as TBCs, which is hypothesized in the latest research [1,2] for the study of thin film spallation. That is, the spallation is driven by pockets of energy concentration and buckling.

4 Conclusion

The life of turbine blades is reduced by the TBC blistering and spallation failures. The blisters nucleate from tiny spots, which has been physically explained by the theory of pockets of energy, and this extra energy beyond the original residual compressive stresses supplies as the blister energy and drive the further growth and spallation. The conventional buckling theory is insufficient to assess TBC spallation process. However, current mechanical models for multilayer material systems lead to excellent agreement with the experimental measurements on the radii for the initiation of unstable growth and spallation of EB-PVD TBC spallation at the room temperature. This novel mechanism can be applied to the assessment of telephone-cord blisters and provides an effective method to determine the interfacial adhesion toughness, mechanical properties for films which are difficult to obtain in experiments.

References

1. Harvey CM, Wang B, Wang S. Spallation of thin films driven by pockets of energy concentration. *Theor. Appl. Fract. Mech.* 92, 1–12 (2017).
2. Wang S, Harvey CM, Wang B. Room temperature spallation of α-alumina films grown by oxidation. *Eng. Fract. Mech.* 178, 401–415 (2017).
3. Tolpygo VK, Clarke DR. Spalling failure of α-alumina films grown by oxidation. II. Decohesion nucleation and growth. *Mater. Sci. Eng. A.* 278(1–2), 151–161 (2000).

4. Tolpygo VK, Clarke DR. Spalling failure of α-alumina films grown by oxidation: I. Dependence on cooling rate and metal thickness. *Mater. Sci. Eng. A.* 278(1–2), 142–150 (2000).
5. Harvey CM, Wang S. Mixed-mode partition theories for one-dimensional delamination in laminated composite beams. *Eng. Fract. Mech.* 96, 737–759 (2012).
6. Wang S, Harvey CM. Mixed mode partition theories for one dimensional fracture. *Eng. Fract. Mech.* 79, 329–352 (2012).
7. Wang S, Harvey C. A theory of one-dimensional fracture. *Compos. Struct.* 94(2), 758–767 (2012).
8. Harvey CM, Wood JD, Wang S, Watson A. A novel method for the partition of mixed-mode fractures in 2D elastic laminated unidirectional composite beams. *Compos. Struct.* 116(1), 589–594 (2014).
9. Wood JD, Harvey CM, Wang S. Partition of mixed-mode fractures in 2D elastic orthotropic laminated beams under general loading. *Compos. Struct.* 149, 239–246 (2016).
10. Hutchinson JW, Suo Z. Mixed Mode Cracking in Layered Materials. In: *Advances in Applied Mechanics*. , 63–191 (1991).
11. Yuan B, Harvey CM, Thomson RC, Critchlow GW, Wang S. A new spallation mechanism of thermal barrier coatings on aero-engine turbine blades. *Theor. Appl. Fract. Mech.* , In press (2018).
12. Zhao X, Wang X, Xiao P. Sintering and failure behaviour of EB-PVD thermal barrier coating after isothermal treatment. *Surf. Coatings Technol.* 200(20–21), 5946–5955 (2006).
13. Liu D, Rinaldi C, Flewitt PEJ. Effect of substrate curvature on the evolution of microstructure and residual stresses in EBPVD-TBC. *J. Eur. Ceram. Soc.* 35(9), 2563–2575 (2015).
14. Busso EP, Qian ZQ, Taylor MP, Evans HE. The influence of bondcoat and topcoat mechanical properties on stress development in thermal barrier coating systems. *Acta Mater.* 57(8), 2349–2361 (2009).
15. Zhao X, Liu J, Rickerby DS, Jones RJ, Xiao P. Evolution of interfacial toughness of a thermal barrier system with a Pt-diffused γ/γ′ bond coat. *Acta Mater.* 59(16), 6401–6411 (2011).
16. Fleck NA, Cocks ACF, Lampenscherf S. Thermal shock resistance of air plasma sprayed thermal barrier coatings. *J. Eur. Ceram. Soc.* 34(11), 2687–2694 (2014).